UNIVERSIDAD DE CONCEPCIÓN

Centro de Investigación en Ingeniería Matemática (CI^{2}MA)

Advance methods of flux identification for Clarifier-Thickener simulation models

Fernando Betancourt, Raimund Bürger,
Stefan Diehl, Camilo Mejías

PREPRINT 2013-15

SERIE DE PRE-PUBLICACIONES

ADVANCED METHODS OF FLUX IDENTIFICATION FOR CLARIFIER-THICKENER SIMULATION MODELS[†]

FERNANDO BETANCOURT[A], RAIMUND BÜRGER[B,*], STEFAN DIEHL[C], AND CAMILO MEJÍAS[B]

Abstract. Mathematical models for the simulation of batch settling and continuous clarifier-thickeners can usually be expressed as a convection-diffusion partial differential equation (PDE). Reliable numerical methods require that the nonlinear flux function of this PDE has been identified for a given material. This contribution summarizes, and applies to experimental data, a recent approach [R. Bürger and S. Diehl, *Inverse Problems* 29 (2013) 045008] for the flux identification in the case of a suspension that shows no compressive behaviour.

The experimental Kynch test and the Diehl test, which are based on an initially homogenous suspension either filling the whole settling column or being initially located above clear liquid, respectively, provide data points that represent a convex and concave, respectively, suspension-supernate interface. A provably convex (concave) smooth approximation of this interface is obtained by solving a constrained least-squares minimization problem. The interface-approximating function can be converted uniquely into an explicit formula for a convex (concave) part of the flux function.

1. Introduction

1.1. **Scope.** This contribution is concerned with mathematical models for the batch and continuous sedimentation of finely divided solid particles dispersed in a viscous fluid. This process is of great importance for the recovery of water utilized in comminution and flotation processes. Since water is a scarce resource in the major part of the Chilean mining zone, one wishes to recover the largest quantity of water possible after the sedimentation process, which generates great interest in mathematical models for the simulation, the design and the control of the unit operation of continuous sedimentation in clarifier-thickener units (cf. Chapter 15 of Wills and Napier-Munn, 2006). Under minor modifications, the same model also describes the operation of so-called secondary settling tanks (SSTs) in wastewater treatment.

Date: June 24, 2013.

Key words and phrases. Solid-liquid separation, thickener simulation, batch sedimentation, flux identification, mathematical model.

[†]Presented at *Computational Modelling '13*, Falmouth, UK, June 18 and 19, 2013.

[*]Corresponding author.

[A]Departamento de Ingeniería Metalúrgica, Facultad de Ingeniería, Universidad de Concepción, Casilla 160-C, Concepción, Chile. E-mail: fbetancourt@udec.cl.

[B]CI[2]MA and Departamento de Ingeniería Matemática, Facultad de Ciencias Físicas y Matemáticas, Universidad de Concepción, Casilla 160-C, Concepción, Chile. E-mail: rburger@ing-mat.udec.cl, cmejias@ing-mat.udec.cl.

[C]Centre for Mathematical Sciences, Lund University, P.O. Box 118, S-221 00 Lund, Sweden. E-Mail: diehl@maths.lth.se.

Reliable spatially one-dimensional simulators are mostly based on the numerical solution of a particular partial differential equation (PDE) of strongly degenerate convection-diffusion type. The solution of this PDE is the local solids volume fraction ϕ as a function of depth and time. The coefficients of the governing PDE rely on two material specific model functions, the so-called Kynch batch flux density function $f_{\mathrm{b}} = f_{\mathrm{b}}(\phi)$ (Kynch, 1952) and the effective solid stress function $\sigma_{\mathrm{e}} = \sigma_{\mathrm{e}}(\phi)$. (The latter is necessary only if the material under study is flocculated.) It is the purpose of this contribution to summarize a new method (recently published in a research paper; Bürger and Diehl, 2013) for the identification of portions of f_{b} from properly designed batch settling tests, and to present new applications of this method to synthetic and measured experimental data.

1.2. **The governing model.** To put the treatment into the proper context, we briefly recall the governing model, focusing here on the simpler case of batch settling in a column of height H. For a derivation of the model and a discussion of its assumptions we refer to Bustos et al. (1999) and Berres et al. (2003). The governing PDE is given by

$$\frac{\partial \phi}{\partial t} - \frac{\partial f_{\mathrm{b}}(\phi)}{\partial x} = \frac{\partial^2 A(\phi)}{\partial x^2}, \tag{1}$$

where ϕ is the sought volumetric solids concentration as a function of time t and height x and f_{b} is the Kynch batch flux density function. The function f_{b} is assumed to be continuous and piecewise differentiable with

$$f_{\mathrm{b}}(0) = f_{\mathrm{b}}(\phi_{\max}) = 0, \quad f_{\mathrm{b}}(\phi) > 0 \quad \text{for } 0 < \phi < \phi_{\max}, \tag{2}$$

where $\phi_{\max}$ is a maximum solids concentration corresponding to a dense-packed sediment. Moreover, the function $A = A(\phi)$ models sediment compressibility in the case that the supension under study is flocculated. This function is also material specific and is given by

$$A(\phi) = \int_0^{\phi} a(s)\,\mathrm{d}s \tag{3}$$

with the integrand

$$a(\phi) := -\frac{f_{\mathrm{b}}(\phi)\sigma_{\mathrm{e}}'(\phi)}{\Delta\varrho g \phi}.$$

Here, $\Delta\varrho$ is the solid density minus the fluid density, g is the acceleration of gravity, and σ_{e}' denotes the derivative of the so-called effective solid stress function $\sigma_{\mathrm{e}} = \sigma_{\mathrm{e}}(\phi)$. This function usually satisfies $\sigma_{\mathrm{e}}(\phi) \geqslant 0$ for all ϕ and

$$\sigma_{\mathrm{e}}'(\phi) := \frac{\mathrm{d}\sigma_{\mathrm{e}}(\phi)}{\mathrm{d}\phi} \begin{cases} = 0 & \text{for } \phi \leqslant \phi_{\mathrm{c}}, \\ > 0 & \text{for } \phi > \phi_{\mathrm{c}}, \end{cases} \tag{4}$$

where $\phi_{\mathrm{c}} > 0$ is a critical concentration or gel point, that is a volume fraction at which the solid particles have physical contact. The assumptions (2) and (4) imply that

$$a(\phi) \begin{cases} = 0 & \text{for } \phi \leqslant \phi_{\mathrm{c}} \text{ and } \phi = \phi_{\max}, \\ > 0 & \text{otherwise}, \end{cases}$$

so (1) is a first-order hyperbolic equation for $\phi \leqslant \phi_c$ and a second-order parabolic equation for $\phi > \phi_c$. Since (1) degenerates to hyperbolic type on a ϕ-interval of positive length, this equation is called *strongly degenerate parabolic*. The location of the suspension-sediment interface where $\phi = \phi_c$, that is the sediment level, is unknown a priori and is part of the solution.

If sediment compressibility is absent, then the right-hand side of (1) is zero and we are reduced to the first-order scalar conservation law of Kynch's theory,

$$\frac{\partial \phi}{\partial t} - \frac{\partial f_b(\phi)}{\partial x} = 0. \tag{5}$$

Following common usage in literature (Bustos et al., 1999), we address suspensions with $A \not\equiv 0$ (i.e., which form compressible sediments) and $A \equiv 0$ (i.e., which obey Kynch's theory) as *flocculated* and *ideal*, respectively.

For the simple case of batch settling of a flocculated or ideal suspension in a column, (1) is supplied with the initial condition

$$\phi(x,0) = \tilde{\phi}_0(x), \quad x \in [0,H], \tag{6}$$

and the zero-flux boundary condition

$$f_b(\phi) + \frac{\partial A(\phi)}{\partial x}\bigg|_{x=x_b} = 0 \quad \text{for } x_b = 0 \text{ and } x_b = H. \tag{7}$$

1.3. **Related work.** The authors have extensively studied a model of continuous sedimentation in clarifier-thickener units that can be expressed by the strongly degenerate convection-diffusion equation

$$\frac{\partial \phi}{\partial t} + \frac{\partial}{\partial z} g(z,\phi) = \frac{\partial}{\partial z}\left(\gamma_1(z)\frac{\partial A(\phi)}{\partial z}\right). \tag{8}$$

Here z denotes a downwards-increasing depth variable varying between an overflow level $z_L < 0$ and an underflow level $z_R > 0$, and at $z = 0$ a feed source is located through which suspension at a feed concentration ϕ_F is fed into the unit. The model involves two discontinuous parameters, γ_1 and γ_2, which are defined by

$$\gamma_1(z) := \begin{cases} 1 & \text{for } z \in (z_L, z_R), \\ 0 & \text{for } z \leqslant z_L \text{ and } z \geqslant z_R, \end{cases} \qquad \gamma_2(z) := \begin{cases} q_L & \text{for } z < 0, \\ q_R & \text{for } z > 0, \end{cases} \tag{9}$$

where $q_L \leqslant 0$ and $q_R \geqslant 0$ are bulk flow velocities that can be controlled externally. The convective flux density function appearing in (8) is given by

$$g(z,\phi) := \gamma_1(z) f_b(\phi) + \gamma_2(z)(\phi - \phi_F). \tag{10}$$

We refer to Betancourt et al. (2013), Bürger and Narváez (2007), Bürger et al. (2004, 2005a, 2005b, 2010, 2011, 2012, 2013) and Garrido et al. (2000, 2003) for a mathematical and numerical analysis of the model (8)–(10) and numerous examples that illustrate that this model provides the basis for realistic thickener simulators. Moreover, the underlying sedimentation-consolidation model of Section 1.2 is equivalent to the suspension dewatering theory employed by Aziz et al. (2000), de Krester et al. (2001), Lester (2002) and Usher et al. (2001), while clarifier-thickener models similar to (8)–(10), and which also rely on the material specific

functions f_b and σ_e or their equivalents, have been studied by several groups of authors including Lev et al. (1986), Barton et al. (1992), Chancelier et al. (1994), Diehl (1996), Bürger et al. (2005a), and Nocoń (2006).

In most of the above-cited works it is assumed that the functions f_b and σ_e for a given suspension under study are known. These model functions are usually determined from batch settling tests. The problem of determining f_b from batch settling tests has been approached in several ways. One approach consists in selecting a global parametric form for f_b, for example the common Richardson and Zaki (1954) formula $f_\mathrm{b}(\phi) = v_0\phi(1-\phi)^{n_\mathrm{RZ}}$ with parameters $v_0 > 0$ and $n_\mathrm{RZ} \geqslant 1$. One then compares an observed temporal or spatial solution profile with a numerically simulated one, and seeks to minimize the distance between both by varying the parameters by employing a descent method (Bürger et al., 2009) or solving an adjoint problem (Coronel et al., 2003), and calculating anew the simulated profile after each variation of the parameters. These techniques are most common for flocculated suspensions (i.e., $A \not\equiv 0$), since in that case, the model (1), (6), (7) usually has no closed-form exact solution.

Kynch's (1952) graphical estimation method does not require the numerical solution of a PDE, nor does the approach of identifying certain observed trajectories with portions of an exact solution and determining the flux parameters by a constrained least-squares technique. For the Kynch test, available treatments include Bueno et al. (1990), Diplas and Papanicolaou (1997), Font and Laveda (2000), Lester et al. (2005) and Grassia et al. (2008, 2011). The graphical method by Kynch utilizes the PDE theory connection between the flux function and the curved discontinuity of the Kynch test. An explicit formula for the estimated flux function in terms of measurable variables was presented by Lester et al. (2005). However, their formula contains an integral over the measured settling velocities. Diehl (2007) presented a simpler formula, which was adopted by Grassia et al. (2008) and is utilized by Bürger and Diehl (2013) and in the present paper to obtain closed-form estimations for f_b.

1.4. **Outline of the paper.** The remainder of this paper is organized as follows. In Section 2 we introduce the batch sedimentation model and tests for the case of an ideal suspension (described by (5), (6)). To this end we recall in Section 2 basic properties of solutions of (5), which are discontinuous in general. In Section 2.2 we discuss the solution of (5), (6) for the Kynch test, that is, for the batch settling of an initially homogeneous suspension in a column. The key issue is that under determined conditions on the initial concentration ϕ_0, this test will produce a suspension-supernate discontinuity that travels with a decreasing speed so that the trajectory is convex in an x versus t plot. The new flux identification method consists in converting an observation of this trajectory into a convex portion of f_b. To improve the possibilities of obtaining information on f_b for $\phi < \phi_\mathrm{infl}$, Diehl (2007) proposed to study a configuration in which the suspension is initially located above a column of clear liquid, from which it is separated by a membrane which is removed at $t = 0$ so that the system is allowed to evolve. This test, the so-called "Diehl test", is described in Section 2.3. Under determined conditions, the suspension-supernate interface produced by this test is concave, and an observation of this interface may be converted into a concave portion of f_b.

Section 3 provides a more detailed description of the flux identification method for the Kynch and Diehl tests. In Section 3.1 an explicit formula for the identified convex portion $\check{f}_\mathrm{b}$

of f_{b} is derived, provided that a convex approximation $\check{h} = \check{h}(t)$ of the suspension-supernate interface is given. The treatment for the concave portion $\hat{f}_{\mathrm{b}}$ arising in the Diehl test is analogous. It is based on a concave approximation $\hat{h} = \hat{h}(t)$ of the suspension-supernate interface, and is outlined in Section 3.2. In Section 3.3 we explain how to generate $\check{h}$. The key issue is the solution of a constrained least-squares optimization problem that provides the coefficients of the piecewise definition of $\check{h}$ as a piecewise cubic, piecewise quadratic or a special piecewise rational function in such a way that $\check{h}$ is once or twice differentiable and convex. The resulting approximation methods are addressed as "spline-fit", "quadratic-fit" and "special-fit", respectively. The generation of $\hat{h}$ in the Diehl test is analogous. Applications of the method are presented in Section 4, considering synthetic data (Section 4.1), one case of experimental data from literature (Section 4.2), and data obtained from a settling experiment of glass beads in glycerine (Section 4.3). Conclusions are collected in Section 5.

2. Batch sedimentation models and tests

2.1. **Properties of solutions of** (5)**.** Solutions of (5), (6) are, in general, discontinuous. If $(t, x(t))$ denotes a trajectory of a discontinuity in the x versus t plane, and at time $t = t_0$ it separates the concentration values ϕ_+ and ϕ_-, then its velocity of propagation is given by the jump condition

$$x'(t)\big|_{t=t_0} = \left.\frac{\mathrm{d}x(t)}{\mathrm{d}t}\right|_{t=t_0} = -\frac{f_{\mathrm{b}}(\phi_+) - f_{\mathrm{b}}(\phi_-)}{\phi_+ - \phi_-}. \tag{11}$$

Since the function f_{b} is nonlinear, discontinuous solutions may arise even from smooth initial data. In the present treatment we assume for simplicity that the function f_{b} has exactly one inflection point, denoted by ϕ_{infl}. Solutions of the problems (5), (6) (and also of (1)–(7)) must be defined as entropy solutions, that is as weak (in general, discontinuous) solutions along with a selection principle, the so-called entropy condition. Roughly speaking, the entropy condition ensures that the solution is physically relevant. In particular it provides a condition of admissibility for discontinuities that separate different solution values. If these conditions are satisfied, then the discontinuity is called a *shock wave* or simply *shock*. If this condition is not satisfied, then a discontinuity posed, for example, in the initial datum must be resolved by a *rarefaction wave*, that is, by a continuous variation of solution values (cf., e.g., Bustos et al., 1999).

2.2. **The Kynch test.** The traditional method of identifying the flux density function f_{b}, the Kynch test, is based on the initial datum

$$\tilde{\phi}_0(x) = \begin{cases} 0 & \text{for } x > H, \\ \phi_0 & \text{for } 0 \leqslant x \leqslant H, \\ \phi_{\max} & \text{for } x < 0, \end{cases} \tag{12}$$

where $\phi_{\max}$ is a maximal concentration and $0 < \phi_0 < \phi_{\max}$ is the homogeneous concentration of the initial suspension. We refer to the solution of the governing equation (1) along with the initial datum (12) as the "Kynch test". If we assume, for simplicity, that the suspension under study is not flocculated, i.e., the governing equation is actually the conservation law (5), then the solution exhibits a descending interface that separates first the suspension

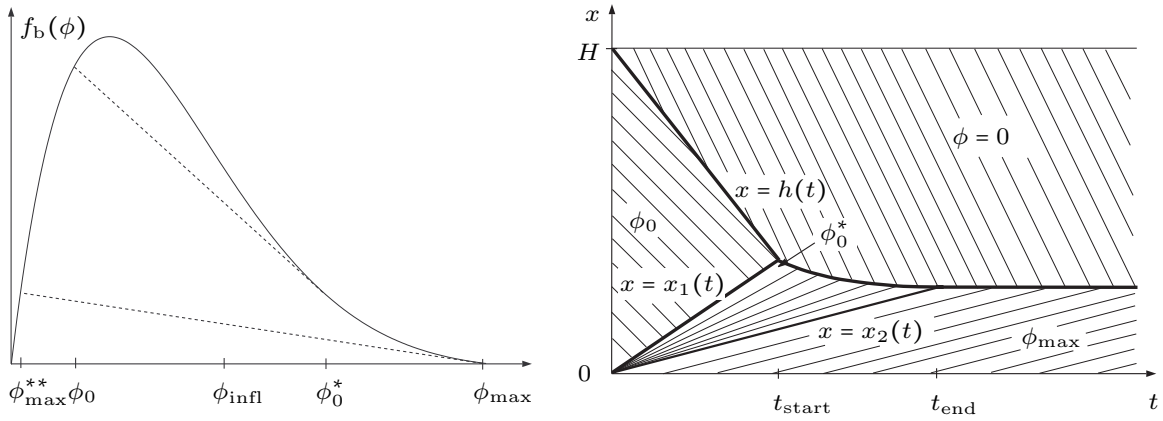

FIGURE 1. Kynch test. Left: plot of the function f_b. The tangent through the point $(\phi_{max}, 0)$ has the slope $f_b'(\phi_{max})$. This tanget intersects the graphs of f_b at a point $\phi^{**}_{max} < \phi_{infl}$. Right: settling plot showing the solution of (5), (6) with the initial datum given by (12), where $\phi_0 \in (\phi^{**}_{max}, \phi_{max}]$. The thin lines are characteristics and the thick lines mark discontinuities, with the exception of x_2, which is a line of continuity.

and then the sediment from the supernatant liquid. On one hand, the height versus time trajectory of this interface can be calculated in closed algebraic form from the curve of f_b versus ϕ, and on the other hand, this interface can easily be observed experimentally. Thus, the trajectory observed for a given material can be converted into a portion of f_b suitable for that material. This property generalizes some well-known methods of thickener design from batch settling tests (Coe and Clevenger, 1916; Kynch, 1952; Talmage and Fitch, 1955; Wilhelm and Naide, 1981).

Roughly speaking, if the initial concentration ϕ_0 is chosen sufficiently large, namely $\phi_0 \in (\phi^{**}_{max}, \phi_{max}]$, where the definition of the value ϕ^{**}_{max} is illustrated in Figure 1, then the Kynch tests permits to reconstruct the portion of f_b for $\phi^*_0 \leqslant \phi \leqslant \phi_{max}$. This information related to the range of high concentrations is usually complemented by the fact that $f_b(0) = 0$, and that for $t \leqslant t_{start}$, the velocity of the descending suspension-supernate interface $x(t) = h(t)$ that separates the values $\phi = 0$ and $\phi = \phi_0$ is according to (11) given by $h'(t) = -f_b(\phi_0)/\phi_0$, which from an observed value of $h'(t)$ allows us to reconstruct the value of $f_b(\phi_0)$. Thus, the Kynch test will provide the functional form of f_b for a certain sub-interval of $[\phi_{infl}, \phi_{max}]$, which is complemented by a small number of pointwise values of f_b for $\phi < \phi_{infl}$.

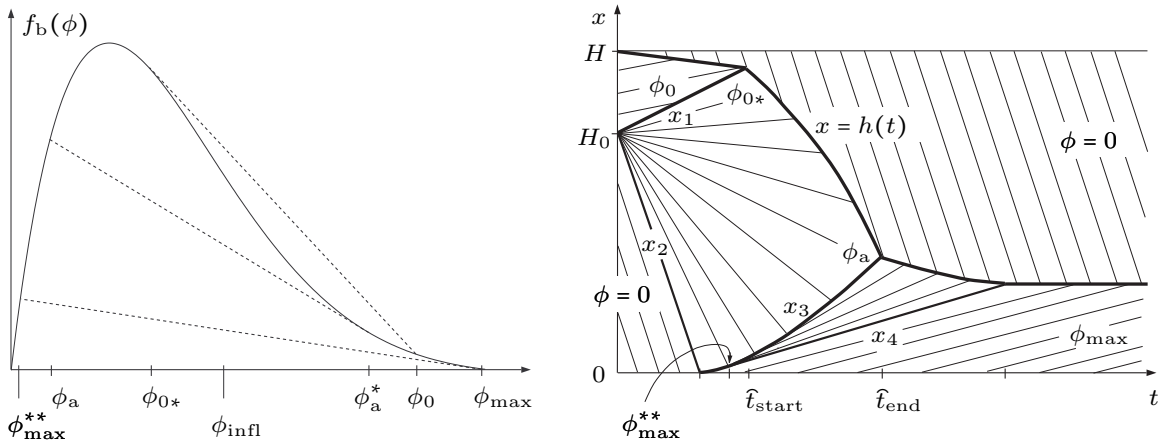

FIGURE 2. Diehl test. Left: the function f_b, showing some of the ϕ-values arising in the solution construction. Right: solution of (5), (6), with initial datum given by (13), for $\phi_0 \in (\phi_{infl}, \phi_{max}]$. The thin lines are characteristics, and the thick lines are discontinuities, with the exception of the line of continuity x_4. The concave trajectory $x = h(t)$, which can be measured in experiments, is a transform of f_b for $\phi \in [\phi_a, \phi_{0*}]$ (Bürger and Diehl, 2013).

2.3. **The Diehl test.** The initial configuration of the Diehl test is represented by

$$\tilde{\phi}_0(x) = \begin{cases} 0 & \text{for } x > H, \\ \phi_0 & \text{for } H_0 \leqslant x \leqslant H, \\ 0 & \text{for } 0 \leqslant x < H_0, \\ \phi_{max} & \text{for } x < 0. \end{cases} \tag{13}$$

Under determined circumstances, the solution of (5), (6), (13) has the following behaviour. The initial supernate-suspension interface located at $x = H_0$, which separates the suspension initially located above the clear liquid, evolves into a rarefaction wave enclosed between an upward-propagating discontinuity (denoted by x_1) and a downward-propagating line of continuity (denoted by x_2; see Figure 2). On the other hand, the interface between the suspension and the supernatant liquid at the top of the suspension, initially located at $x = H$, moves downwards (in the special case $\phi_0 = \phi_{max}$, it is standing still). At some moment, denoted by $\hat{t}_{start}$, this interface and x_1 will meet. At that time, the initial concentration ϕ_0 disappears, and the interface separating the suspension from the supernatant clear liquid becomes a shock $x = h(t)$, which is curved since the characteristics emerging at $x = H_0$ form a rarefaction wave. It is precisely this concave interface $x = h(t)$ that will be used for the identification of a segment of f_b. This segment ranges from $\phi = \phi_{0*}$ to $\phi = \phi_a$, where $\phi_{0*} < \phi_{infl}$ is the ϕ-value such that the tangent to the graph of f_b through $(\phi_{0*}, f_b(\phi_{0*}))$ intersects the graph of f_b in $(\phi_0, f_b(\phi_0))$, and ϕ_a is a limiting value that depends on the accumulation of sediment on the bottom of the unit (see Figure 2). For details we refer to Diehl (2007).

3. The problem of flux identification

3.1. **Rarefaction waves and curved trajectories in the Kynch test.** As is stated above, the key motivation of the present approach is the fact that a function f_b, which for the moment we assume to possess one inflection point only, and for an appropriately chosen value of ϕ_0, the trajectory $(t, h(t))$ is the transform of a segment of the curve $(\phi, f_\mathrm{b}(\phi))$ for certain values of ϕ with $\phi > \phi_\mathrm{infl}$ (in the case of the Kynch test, see Figure 1) or $\phi < \phi_\mathrm{infl}$ (in the case of the Diehl test (13), see Figure 2), and that in an x versus t diagram, the mentioned trajectory is either convex (in the case of (12)) or concave (for (13)).

To be explicit, let us concentrate for the moment on the Kynch test, and define the function

$$\eta(t) := h(t) - th'(t), \tag{14}$$

where $h(t)$ denotes the time-dependent position of the suspension-supernate interface, which eventually becomes the sediment-supernate interface. (Note that if we draw this interface in an x versus t settling plot, then $\eta(t)$ is the intercept between the tangent to h going through the point $(t, h(t))$ with the x-axis.) One can then prove that the interface trajectory $h(t)$, the values ϕ asssumed within the rarefaction fan originating in $(x = 0, t = 0)$, and the corresponding values $f_\mathrm{b}(\phi)$ are related by the pair of equations

$$\phi = \frac{H\phi_0}{\eta(t)}, \quad f_\mathrm{b}(\phi) = -\frac{H\phi_0}{\eta(t)}h'(t) \quad \text{for } t_\mathrm{start} \leqslant t \leqslant t_\mathrm{end}. \tag{15}$$

If $h(t)$ is convex, that is $h''(t) > 0$ for $t_\mathrm{start} \leqslant t \leqslant t_\mathrm{end}$, then η is an invertible function of t and we may eliminate t from (15) to obtain the explicit formula

$$f_\mathrm{b}(\phi) = -\phi h'\left(\eta^{-1}\left(\frac{H\phi_0}{\phi}\right)\right) \quad \text{for } \phi_0^* \leqslant \phi \leqslant \phi_\mathrm{max}, \tag{16}$$

where $\phi_0^* = H\phi_0/\eta(t_\mathrm{start})$. This property forms the basis of the flux identification method in the present work, which is based on the mathematically rigorous exposition by Bürger and Diehl (2013). The basic idea is the following: suppose that measurements of the interface $h(t)$ are available, which may be affected by noise. Moreover, assume that we have at hand a smooth curve $\check{h}(t)$, which is convex and which may be defined as a spline curve (that is, as a twice differentiable curve defined in a piecewise sense by cubic polynomials), as a differentiable, piecewise parabolic or as a twice differentiable, piecewise rational function. (In what follows, these three alternatives will be addressed as "spline-fit", "quadratic-fit" and "special-fit" methods, respectively.) Then we may reconstruct a segment of f_b, denoted here by $\check{f}_\mathrm{b}$, by using the function $\check{h}'$ instead of h' in (14) and (16). That is, if $\check{h}''(t) \geqslant 0$ for $t_\mathrm{start} \leqslant t \leqslant t_\mathrm{end}$, then we define

$$\check{\eta}(t) = \check{h}(t) - t\check{h}'(t) \quad \text{for } t_\mathrm{start} \leqslant t \leqslant t_\mathrm{end}, \tag{17}$$

and by inverting $\check{\eta}$ (which is possible in closed algebraic form for the spline-fit, quadratic-fit and special-fit methods), we may recover the desired segment of f_b via

$$\check{f}_\mathrm{b}(\phi) = -\phi\check{h}'\left(\check{\eta}^{-1}\left(\frac{H\phi_0}{\phi}\right)\right) \quad \text{for } \phi_0^* \leqslant \phi \leqslant \phi_\mathrm{max}. \tag{18}$$

In the case f_b has several inflection points, the parametric and explicit representations of the flux function, (15) and (16), still hold. The set of ϕ is always a subset of the convex parts

of f_{b}. In case f_{b} has three inflection points, this set may consist of two disjoint intervals corresponding to the "convex hull" construction for rarefaction waves for this type of PDE.

3.2. **Rarefaction waves and curved trajectories in the Diehl test.** Although the solution of a Diehl test (see Figure 2) is substantially different from that of the Kynch test, it also has (during the time interval between t_{start} and t_{end}) an expansion wave below the supernate-suspension interface $x = h(t)$; however, this interface is *concave*. The concentrations in this expansion wave lie in an interval the left of the inflection point ϕ_{infl} where the flux function is concave. The derivation of the following formulas is similar to the case of the Kynch test (Diehl, 2007):

$$\phi = \frac{(H - H_0)\phi_0}{\eta(t) - H_0}, \quad f_{\mathrm{b}}(\phi) = -\frac{(H - H_0)\phi_0}{\eta(t) - H_0} h'(t) \quad \text{for } t_{\mathrm{start}} \leqslant t \leqslant t_{\mathrm{end}}, \tag{19}$$

where η is defined by (14). If $h(t)$ is concave, that is $h''(t) < 0$ for $t_{\mathrm{start}} \leqslant t \leqslant t_{\mathrm{end}}$, then η is an invertible function of t and we may eliminate t from (19) to obtain the explicit formula

$$f_{\mathrm{b}}(\phi) = -\phi h' \left(\eta^{-1} \left(H_0 + \frac{(H - H_0)\phi_0}{\phi} \right) \right) \quad \text{for } \phi_{\mathrm{a}} \leqslant \phi \leqslant \phi_{0*},$$

where $\phi_{\mathrm{a}} = (H - H_0)\phi_0/(\eta(t_{\mathrm{end}}) - H_0)$.

3.3. **Convex and concave approximations of measured interfaces.** We now provide more technical detail on the determination of the convex approximation $\check{h}(t)$ of the suspension-supernate interface for the Kynch test. The procedure is analogous for the Diehl test and we omit the details here. Assume that the raw data is a collection of N points

$$(t_j, x_j), \quad j \in \{j_1 := 1, \ldots, j_2, \ldots, j_3, \ldots, j_n, \ldots, j_{n+1} := N\}, \tag{20}$$

which represent measurements of the sediment-supernate interface $x = h(t)$ (see Figure 1) for the time interval $t \in [t_{\mathrm{start}}, t_{\mathrm{end}}]$. We assume that each interval $(t_{j_i}, t_{j_{i+1}}]$ contains $N_i := j_{i+1} - j_i$ points, such that $N = 1 + N_1 + \cdots + N_n$. One then determines smooth functions $\check{h}_i$, $i = 1, \ldots, n$, which approximate these data in such a way that the function

$$\check{h}(t) := \sum_{i=1}^{n} \check{h}_i(t)\chi_i(t), \quad t_1 < t \leqslant t_N, \tag{21}$$

which is defined in a piecewise manner through the indicator functions

$$\chi_i(t) := \begin{cases} 1 & \text{if } t_{j_i} < t \leqslant t_{j_{i+1}}, \\ 0 & \text{otherwise,} \end{cases}$$

is smooth and convex. It is ensured that the function $\check{h}$ is smooth (for instance, once or twice differentiable) if we employ one of the following methods:

(1) the *spline-fit method*, for which we employ on each interval the approach

$$\check{h}_i(t) = a_i t^3 + b_i t^2 + c_i t + d_i, \quad i = 1, \ldots, n \tag{22}$$

with coefficients a_i, b_i, c_i and d_i which are determined in such a way that the resulting curve $\check{h}(t)$ is twice differentiable,

(2) the *quadratic-fit method*, for which we employ on each interval the approach

$$\check{h}_i(t) = a_i t^2 + b_i t + c_i, \quad i = 1, \ldots, n \tag{23}$$

with coefficients a_i, b_i and c_i which are determined in such a way that the resulting curve $\check{h}(t)$ is differentiable,

(3) or the *special-fit method*, for which we employ on each interval the approach

$$\check{h}_i(t) = \frac{a_i}{t^2} + \frac{b_i}{t} + c_i + d_i t, \quad i = 1, \ldots, n \tag{24}$$

with coefficients a_i, b_i, c_i and d_i which are determined in such a way that the resulting curve $\check{h}(t)$ is twice differentiable.

The determination of the coefficients for each of the functional forms (22), (23) and (24) so that the resulting curve $\check{h}$ is the best approximation of the data (20) and at the same time the smoothness requirements are met is a standard least-squares approximation (quadratic programming) problem. However, we here require that in addition the function $\check{h}$ be convex (for the case of the Kynch test), i.e., we request that $\check{h}'' \geqslant 0$. This requirement further restricts the possible values of the coefficients $a_i, \ldots, d_i$.

To formalize the description of the resulting constrained quadratic programming problem, we first note that $\check{h}_i(t) = \boldsymbol{q}(t)^{\mathrm{T}} \boldsymbol{p}_i$ for $i = 1, \ldots, n$, where we define $\boldsymbol{p}_i := (a_i, b_i, c_i, d_i)^{\mathrm{T}}$ and the vector function

$$\boldsymbol{q}(t)^{\mathrm{T}} := \begin{cases} (t^3, t^2, 1, 1) & \text{for the spline-fit method (22),} \\ (t^2, t, 1, 0) & \text{for the quadratic-fit method (23),} \\ (1/t^2, 1/t, 1, t) & \text{for the special-fit method (24).} \end{cases}$$

Furthermore, we define the vectors

$$\boldsymbol{p} := \begin{pmatrix} \boldsymbol{p}_1 \\ \boldsymbol{p}_2 \\ \vdots \\ \boldsymbol{p}_n \end{pmatrix}, \quad \boldsymbol{x}_i := \begin{pmatrix} x_{j_i} \\ x_{j_i+1} \\ \vdots \\ x_{j_{i+1}-1} \end{pmatrix}, \quad \boldsymbol{x} := \begin{pmatrix} \boldsymbol{x}_1 \\ \boldsymbol{x}_2 \\ \vdots \\ \boldsymbol{x}_n \\ x_N \end{pmatrix},$$

where $\boldsymbol{p}$ is the vector of unkwowns, that is, of the coefficients in (22), (23) or (24) that determine the shape of (21). The vector $\boldsymbol{p}$ is determined as the solution of the following constrained quadratic programming problem:

$$\begin{aligned} &\text{minimize } J(\boldsymbol{p}) = (\boldsymbol{Q}\boldsymbol{p} - \boldsymbol{x})^{\mathrm{T}} (\boldsymbol{Q}\boldsymbol{p} - \boldsymbol{x}) \\ &\text{subject to the regularity condition } \boldsymbol{R}^{\text{method}} \boldsymbol{p} = \boldsymbol{0} \\ &\text{and the convexity condition } \boldsymbol{I}^{\text{method}} \boldsymbol{p} \leqslant \boldsymbol{b}^{\text{method}}, \end{aligned} \tag{25}$$

where $\boldsymbol{Q}$ denotes the matrix

$$\boldsymbol{Q} := \begin{bmatrix} \boldsymbol{Q}_1 & \boldsymbol{0} & \cdots & \boldsymbol{0} \\ \boldsymbol{0} & \boldsymbol{Q}_2 & \ddots & \vdots \\ \vdots & \ddots & \ddots & \boldsymbol{0} \\ \boldsymbol{0} & \cdots & \boldsymbol{0} & \boldsymbol{Q}_n \\ \boldsymbol{0} & \ddots & \boldsymbol{0} & \boldsymbol{q}(t_N)^{\mathrm{T}} \end{bmatrix},$$

where in turn we define

$$\boldsymbol{Q_i} := \begin{bmatrix} \boldsymbol{q}(t_{j_i})^{\mathrm{T}} \\ \boldsymbol{q}(t_{j_i+1})^{\mathrm{T}} \\ \vdots \\ \boldsymbol{q}(t_{j_{i+1}-1})^{\mathrm{T}} \end{bmatrix}, \quad i = 1, \ldots, n,$$

and $\boldsymbol{R}^{\text{method}}$ and $\boldsymbol{I}^{\text{method}}$ are certain given matrices and $\boldsymbol{b}^{\text{method}}$ is a given vector, where the superscript "method" indicates that the respective quantity depends on the choice of the method (spline-fit, quadratic-fit or special-fit). The inequality in $\boldsymbol{I}^{\text{method}}\boldsymbol{p} \leqslant \boldsymbol{b}^{\text{method}}$ is understood in the component-wise sense. The precise expressions are all given by Bürger and Diehl (2013), where it is also proven that the problem (25) always has a unique solution. To illustrate the main idea, we provide in the Appendix further detail for the particularly transparent case of the quadratic-fit (23).

4. Application to synthetic and experimental data

In this section, we analyze data from three different suspensions partly to demonstrate the methods and partly to investigate which of the methods of identification (spline-fit, quadratic-fit or special-fit) is preferable in each case. To this end, we note first that the number n of subintervals of $\check{h}(t)$, $\check{\eta}(y)$ and $\check{f}_{\mathrm{b}}(\phi)$ can be chosen arbitrarily provided that $n < N/4$. While for a chosen method the accuracy of the identification method, measured by the smallness of J defined in (25), usually increases when n is increased, for the application of available solvers for the constrained quadratic programming problem (25) and the ease of implementation of simulators of continuous sedimentation it is desirable that n is chosen as small as possible.

4.1. Application to synthetic data.

Here, we analyze data obtained by numerical simulation of the governing PDE (1) with and without the presence of the compressive term $A(\phi)_{xx}$ on the right-hand side. The following constitutive functions have been obtained from experimental measurements on Chilean copper ore tailings by Becker (1982), and have been used in a number of previous works (see, e.g., Bustos et al., 1999 and Bürger and Narváez, 2007):

$$f_{\mathrm{b}}(\phi) = \begin{cases} v_0\phi(1-\phi)^{12.59} & \text{for } 0 \leqslant \phi \leqslant 1, \\ 0 & \text{otherwise,} \end{cases}$$

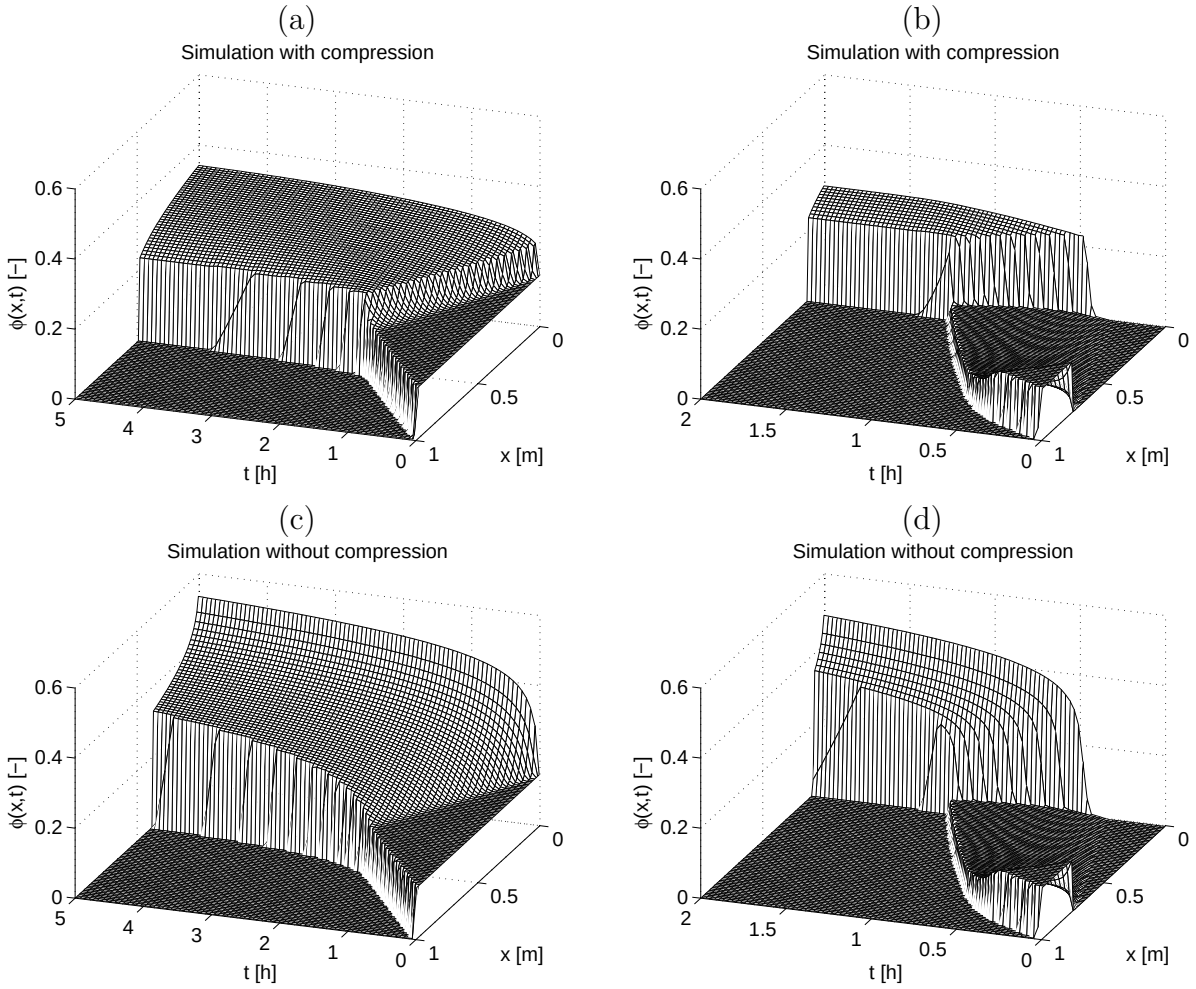

FIGURE 3. Numerical simulations of the Kynch and Diehl tests (a, b) with compression present, (c, d) without compression.

$$\sigma_{\mathrm{e}}(\phi) = \begin{cases} 0 & \text{for } \phi \leqslant \phi_{\mathrm{c}} := 0.23, \\ \sigma_0 \exp(17.9\phi) & \text{for } \phi > \phi_{\mathrm{c}}, \end{cases}$$

where $v_0 = 0.000605\,\mathrm{m/s}$ and $\sigma_0 = 5.35\,\mathrm{Pa}$. For the compression function (3) we also have $\Delta\varrho_{\mathrm{s}} = 1650\,\mathrm{kg/m^3}$ and $g = 9.81\,\mathrm{m/s^2}$. A graph of the flux function f_{b} is drawn as the black dashed curve in Figure 6 (b). The inflection point of f_{b} is $\phi_{\mathrm{infl}} = 2/(1 + 12.59) \approx 0.1472$. Since the theoretically maximal intervals of ϕ for the identification with the Kynch and Diehl tests are obtained with $\phi_0 = \phi_{\mathrm{infl}}$, we choose this initial value for the numerical simulations here; see Figures 3 (a) and (b). In Figures 3 (c) and (d), the same tests are simulated without the compression function present, i.e., σ_0 has been set to zero.

Since compression is only present in the solution wherever ϕ exceeds the critical concentration $\phi_{\mathrm{c}} = 0.23$, the Diehl test yields the same solution with and without compression for the major part of the concave interface; see Figures 3 (b) and (d). This means that the

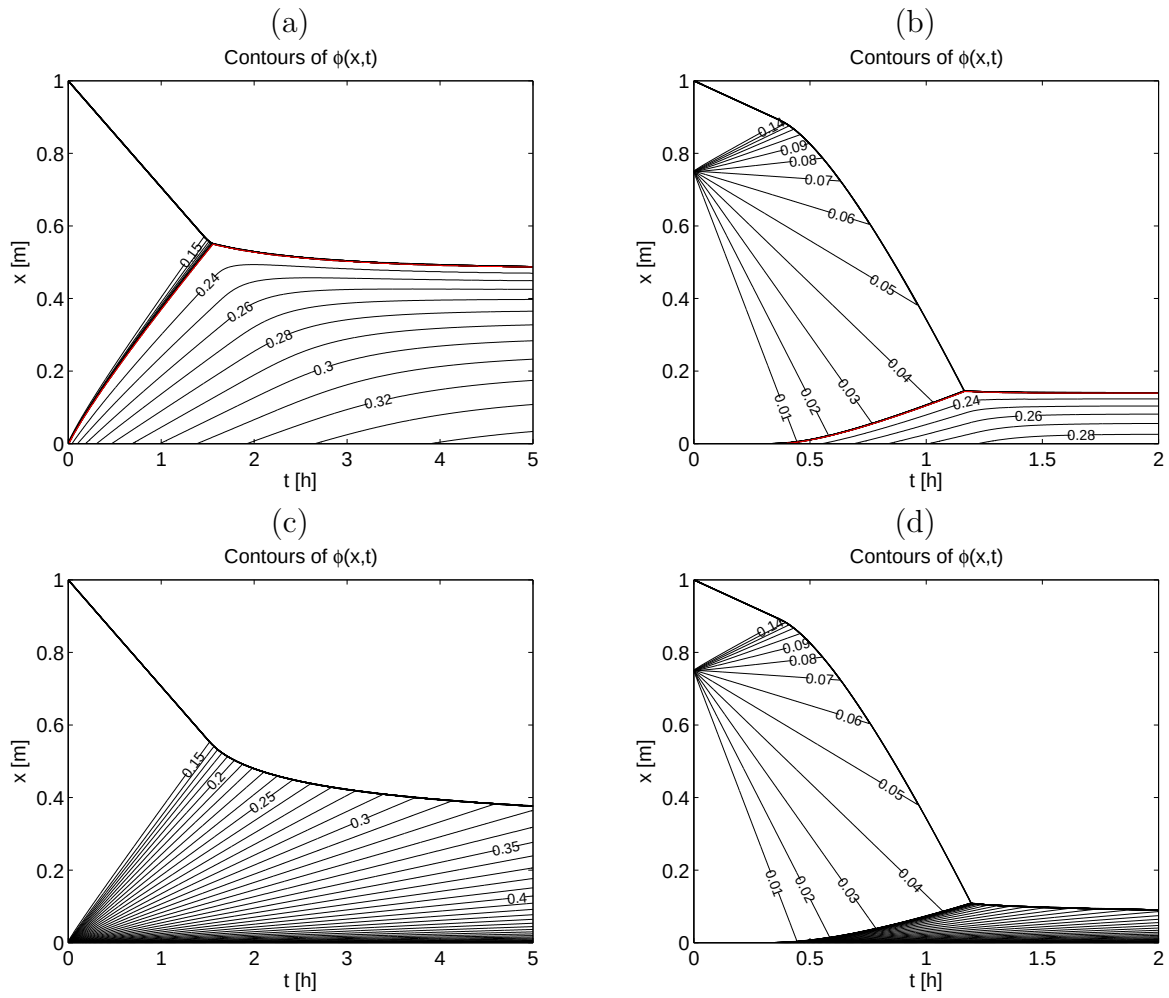

FIGURE 4. Contours (iso-concentration curves) of the simulations (a, b) shown in Figures 3 (a) and (b) (with compression) and (c, d) shown in Figure 3 (c) and (d) (without compression). The contours correspond to ϕ-values that are multiples of 0.01. The thin red line in plots (a) and (b) refers to the critical concentration $\phi_c = 0.23$.

accurate identification method can be used for a Diehl test also for flocculated suspensions as long as $\phi_0 < \phi_c$. In Figure 4 the contours of the simulations are shown during a longer time interval.

We now apply the identification method to the curved interfaces in Figure 4. From these synthetically produced interfaces, several points are obtained by clicking with the mouse on the computer screen. This introduces some noise to the data. To assess which fitting method and what number of subintervals will give good fits, we display the results of several runs in Figure 5.

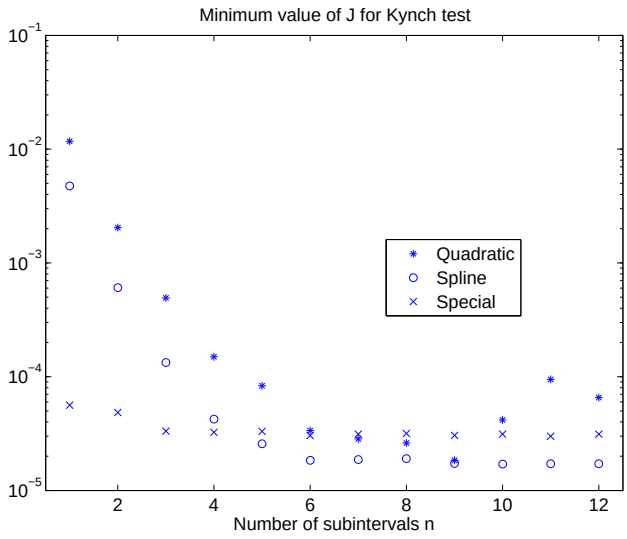

FIGURE 5. Values of J in the minima of the optimization problem (25) for the Kynch test for different numbers of n for the synthetic data of Figure 4 (c).

Based on Figure 5, we perform the special-fit method for one interval, see Figures 6 (a) and (b), and the spline-fit method with four subintervals, see Figures 6 (c) and (d). The subintervals are marked by the vertical dashed blue lines.

For the Diehl test, Figure 7 shows the quality of the different fits with different numbers of subintervals. In Figures 8 (a) and (b), we show the result of a special-fit with one interval and in Figures 8 (c) and (d) a fit with five segments.

Note that the special-fit method, see Figure 8 (b), results in an estimated concave part of the flux function, which goes above the inflection point $\phi_{\text{infl}} \approx 0.1472$, whereas the spline-fit method is more accurate; see Figure 8 (d).

4.2. **Application to experimental data from literature.** There are many published experiments of the Kynch test. Here we choose those reported by Karamisheva and Islam (2005) in their Figure 2; see Figure 9 (a) and (c). Four Kynch tests were performed with activated sludge from a municipal wastewater treatment plant and with the initial concentrations $\phi_0 = 1.6$, 2.4, 3.7 and 7.2 g/l.

By inspection of the data points in Figure 9 (a) or (c), we first choose the time point t_{start}, to the left of which we fit a straight line. The (magnitude of the) slope of this line gives an estimation of the settling velocity of the corresponding initial concentration; see the coloured circles in Figure 9 (b) and (d).

The limited number of data points to the right of t_{start} representing the convex part of $h(t)$ seen in Figure 9 (a) and (c), and the requirement to have a unique solution to the optimization problem imply that we use only one or two subintervals for the different fits. Since there are different numbers of data points in each of the four tests, we normalize the errors as follows. Let J denote the value of the functional corresponding to the solution of (25) for a fixed n. For the test with $\phi_0 = 1.6$ g/l with the number of data points $N_{1.6} = 11$ we set $J_{1.6} := J/N_{1.6}$ and do the corresponding for the other three tests. Then we define the

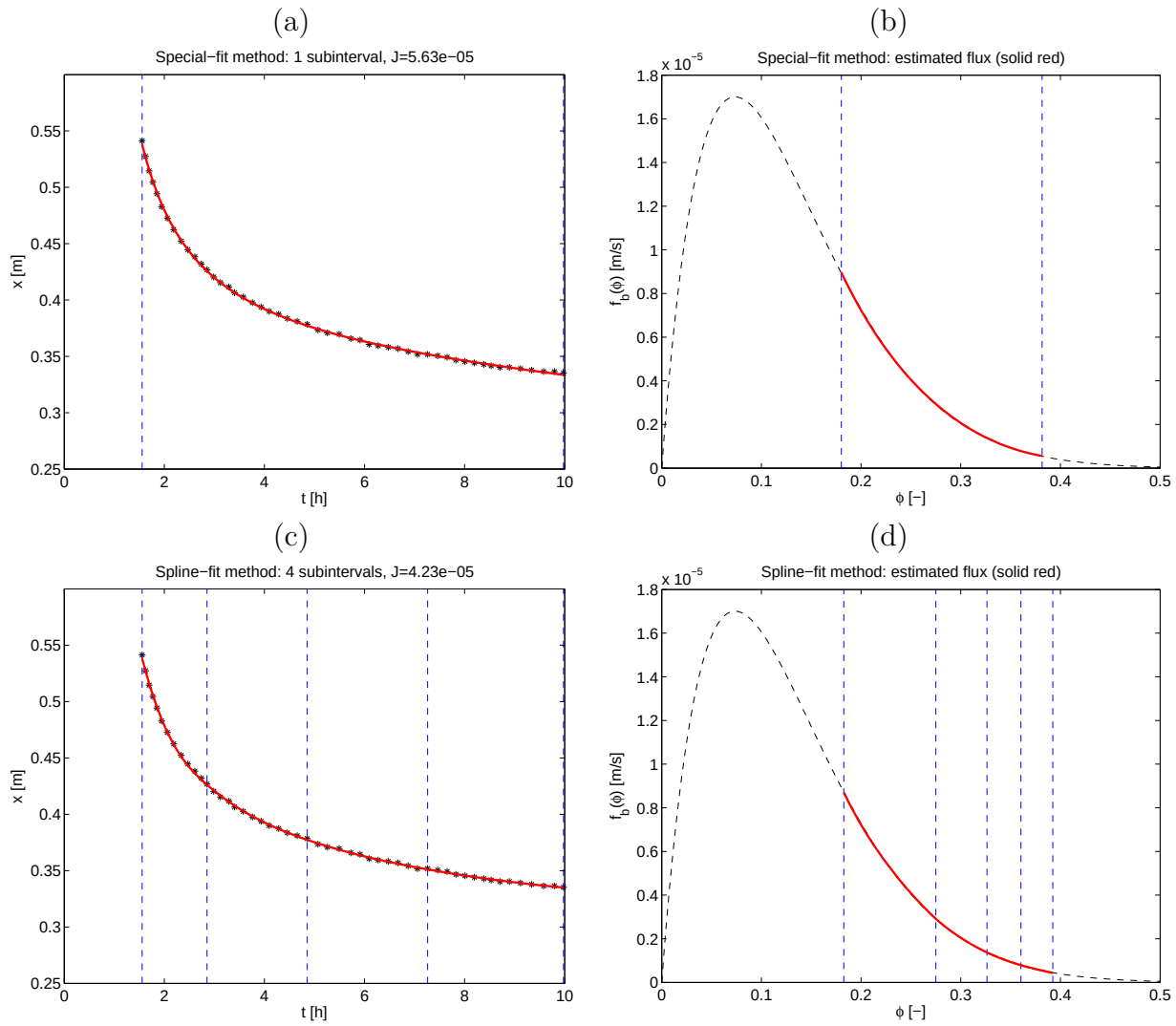

FIGURE 6. (a, b) Special-fit method, (c, d) spline-fit method, both applied to the synthetic data of Figure 4 (c).

average $J_{\text{total}} := (J_{1.6} + J_{2.4} + J_{3.7} + J_{7.2})/4$ as a measure of how good the fit is. The values of J_{total} for the three methods are $J_{\text{total}} = 0.49378$, 0.22054 and 0.03515 for the quadratic-fit, spline-fit, and special-fit methods, respectively, for $n = 1$ subinterval, and $J_{\text{total}} = 0.03854$, 0.01502, and 0.035082 for each of these methods, respectively, for $n = 2$ subintervals. The best fit for $n = 1$ is obtained with the special method; cf. Figure 9 (a)–(b), and the best fit for $n = 2$ is obtained with spline segments; cf. Figure 9 (c)–(d).

4.3. **Application to experimental data.** To further provide experimental support for the flux identification method, settling experiments of a suspension of glass beads were conducted by using the SediRack equipment. SediRack is an equipment that permits one to conduct five settling experiments at different initial concentrations simultaneously, see

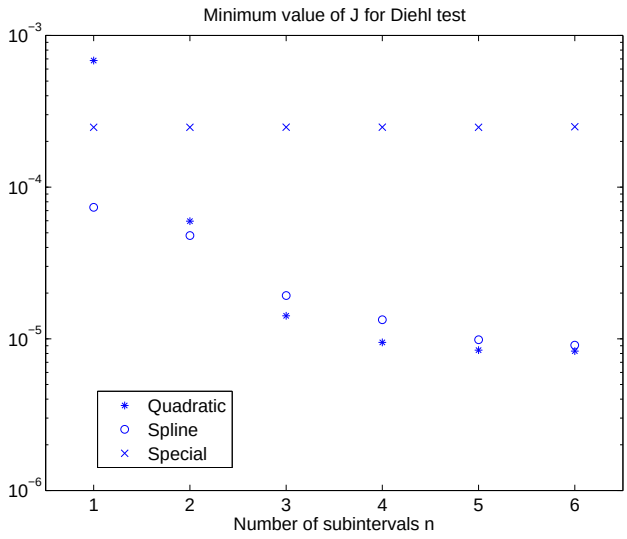

FIGURE 7. Values of J in the minima of the optimization problem (25) for the Diehl test for different numbers of n for the synthetic data of Figure 4 (d).

Figure 10 (a). The settling columns are mounted into a frame that can be rotated to create an initially homogeneous suspension in each of the columns. A videocamera observes the settling process. By using a special image processing software installed in a notebook one can eventually record the suspension-supernate interface of in each of the columns as a function of time (see Figure 10). This is precisely the kind of information the present flux identification method can be applied to. Some results are shown in Figures 11–13.

For the experiments we used technical quality glass beads (manufactured by Potters Industries, Inc., Carlstadt, New Jersey), U.S. screen number 20–30 of density $\varrho_s = 4210\,\mathrm{kg/m^3}$. The liquid utilized was a solution of industrial glycerine and distilled water of volumetric concentration 0.95 in glycerine, density $\varrho_f = 1247\,\mathrm{kg/m^3}$ and viscosity $0.3469\,\mathrm{Pa\,s}$. The solution viscosity was measured with a viscometer Rotovisco RV-20 (Haake). The experimental procedure consisted in (i) preparing the solid particles to obtain the required concentration in each tube, (ii) introducing the particle charges into each tube, (iii) filling each tube with the solution up to the height of $H = 287\,\mathrm{mm}$, (iv) closing the cover, (v) rotating the tubes as many times as necessary to obtain a homogeneous suspension, (vi) fastening the frame and (vii) starting the data acquisition in the notebook. The software gives the possibility of selecting the sample time interval. For all experiments the sample time interval 1 s was chosen. Temperature was recorded in each run and ranged from 21 °C to 23 °C.

To assess which of the methods would provide the best flux approximation for the available experimental data and a given number of subintervals n, we now define the functional J for each fixed number n of subintervals as the average of the four tests that have rarefaction waves normalized with the number of data points N, i.e., we define for the run with $\phi_0 = 0.268$

$$J_{268} := \frac{(\boldsymbol{Qp} - \boldsymbol{x})^{\mathrm{T}}(\boldsymbol{Qp} - \boldsymbol{x})}{N_{268}}.$$

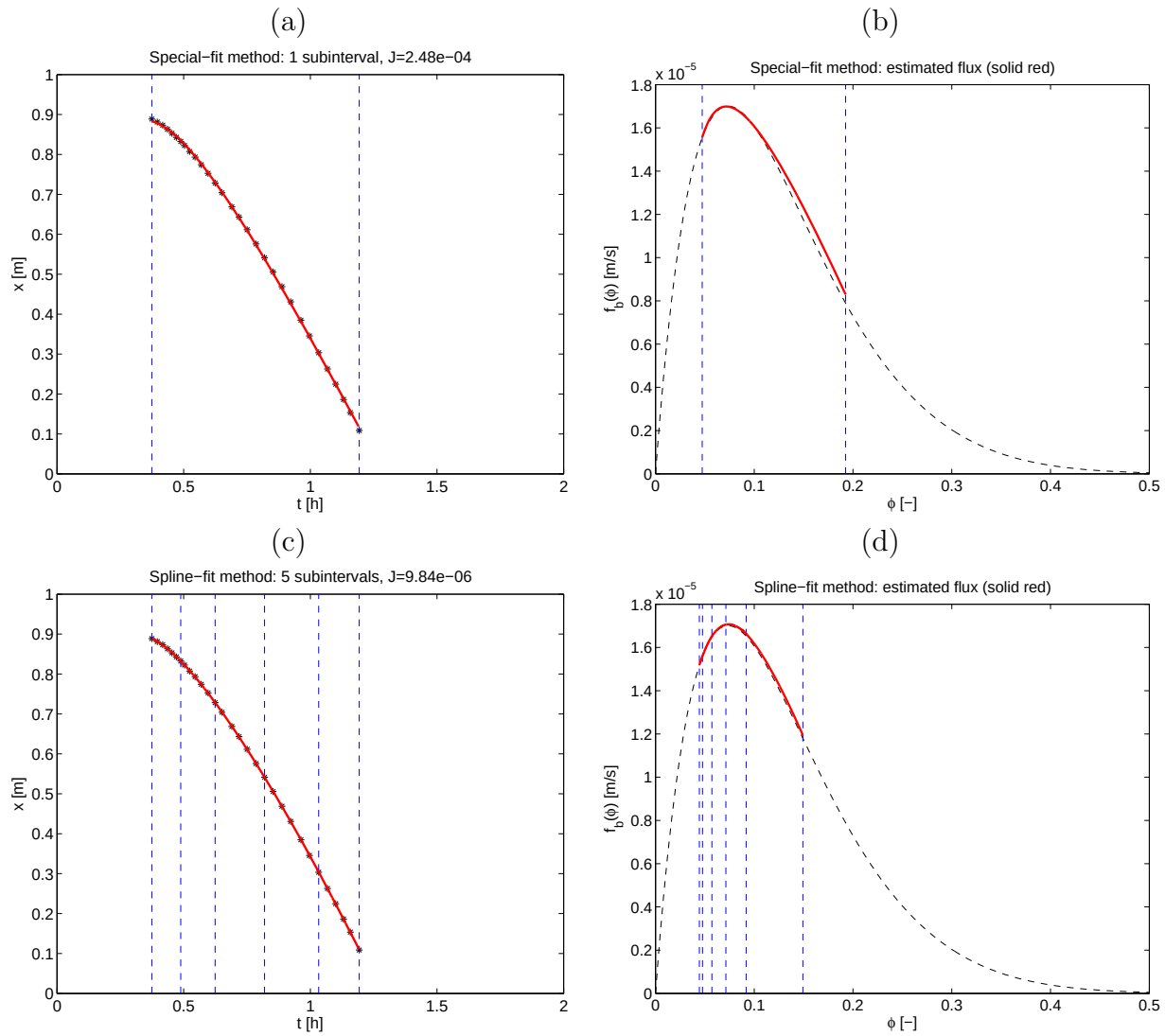

FIGURE 8. (a, b) Special-fit method and (c, d) spline-fit method, both applied to the synthetic data of Figure 4 (d).

Define in analogous manner J_{298}, J_{318} and J_{338}, and calculate $J_{\text{total}} = (J_{268} + J_{298} + J_{318} + J_{338})/4$. The minima of the quantities J_{total} obtained in this way are plotted for the three methods proposed (spline-fit, quadratic-fit and special-fit) in Figure 14. This plot informs that for $n = 1$, the spline-fit method gives the smallest minimum of J_{total}, while for $n = 2, \ldots, 30$ the smallest value is attained for the quadratic-fit method.

5. Conclusions

The three identification methods (spline-fit, quadratic-fit or special-fit) have been applied on three sets of suspensions and data:

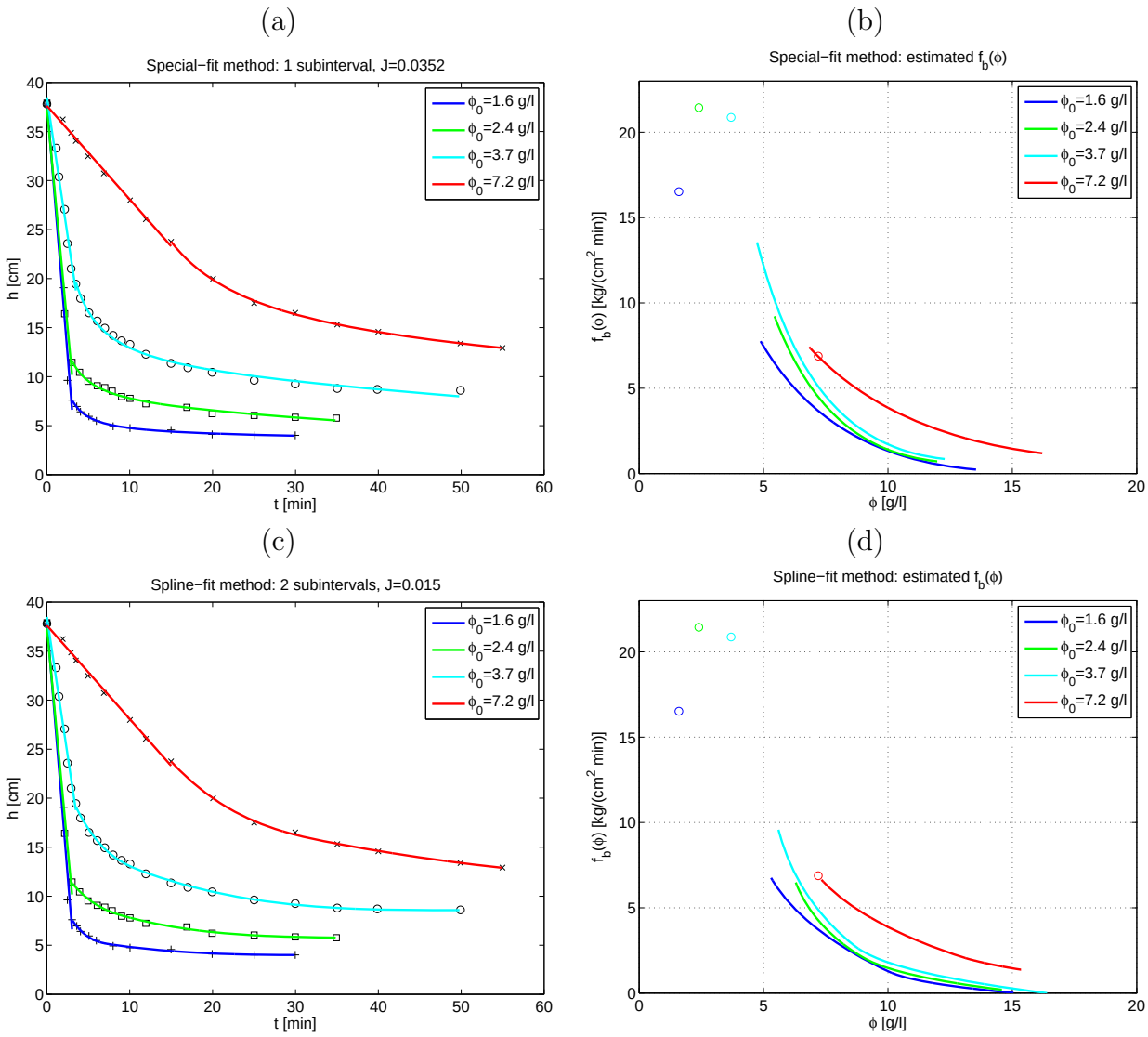

FIGURE 9. The black markers in (a) and (c) show the data of four Kynch tests from Karamisheva and Islam (2005). The coloured lines show the results of: (a)–(b) the special-fit method with one interval; (c)–(d) the spline-fit method with two subintervals.

(1) Synthetically produced data with a flux function measured from experimental data of copper ore tailings (Section 4.1). For the identification of the convex part of the flux function from a Kynch test, the special-fit method is then sufficiently accurate already with only one subinterval; see Figures 6 (a) and (b). A concave part of the flux can be identified from the Diehl test, but then several spline segments should be used for a sufficiently accurate result; see Figures 8 (c) and (d).
(2) Published data by Karamisheva and Islam (2005): Four Kynch tests of activated sludge from a wastewater treatment plant have resulted in similar flux estimations

(a) (b)

FIGURE 10. (a) SediRack equipment, (b) snapshot of suspension-supernate interfaces measured by SediRack.

by either the special-fit method with one interval, or the spline-fit method with two intervals: see Figure 9.

(3) Newly conducted Kynch tests of glass beads in 95% glycerine. For this suspension, it is interesting to note that the quadratic-fit method gives the best fit for two or more subintervals; see Figure 14.

In agreement with the results of the analysis of the synthetically produced data in Bürger and Diehl (2013), the two first suspensions here show that the minimum values of J for the spline-fit are consistently smaller than those for the quadratic-fit method. These findings sharply contrast with our experiments with glass beads; see Figure 14. For this suspension and the Kynch test, the special-fit produces non-small minimal values of J that are nearly constant for all n. More interestingly, only for $n = 1$ does the spline-fit produce the best approximation, while for $n \geq 2$ the quadratic-fit yields significantly smaller minimal values of J. The reason for this is that there are no constraints on the second derivative in the optimization with the quadratic-fit as there are with the spline-fit and special-fit methods. According to Theorem 2.1 of Bürger and Diehl (2013), this means that the resulting estimated portion of the flux is only once continuously differentiable. Generally, the quadratic-fit method can only give once continuously differentiable functions h and f_{b}, whereas the spline-fit and special-fit yield twice continuously differentiable functions h and f_{b}.

The comparison between the results above shows that glass beads produce a completely different behaviour than the other suspensions. Thus, one cannot generically single out one of the methods (spline-fit, quadratic-fit or special-fit) in favor of the two others. Rather, all three methods should be investigated for each material. For instance, for the quadratic-fit method with $n = 1$ (sub-)interval for the case $\phi_0 = 0.338$, the coefficients of (23) are

$$a_1 = 6.9318 \times 10^{-4}, \quad b_1 = -0.6225, \quad c_1 = 286.9567.$$

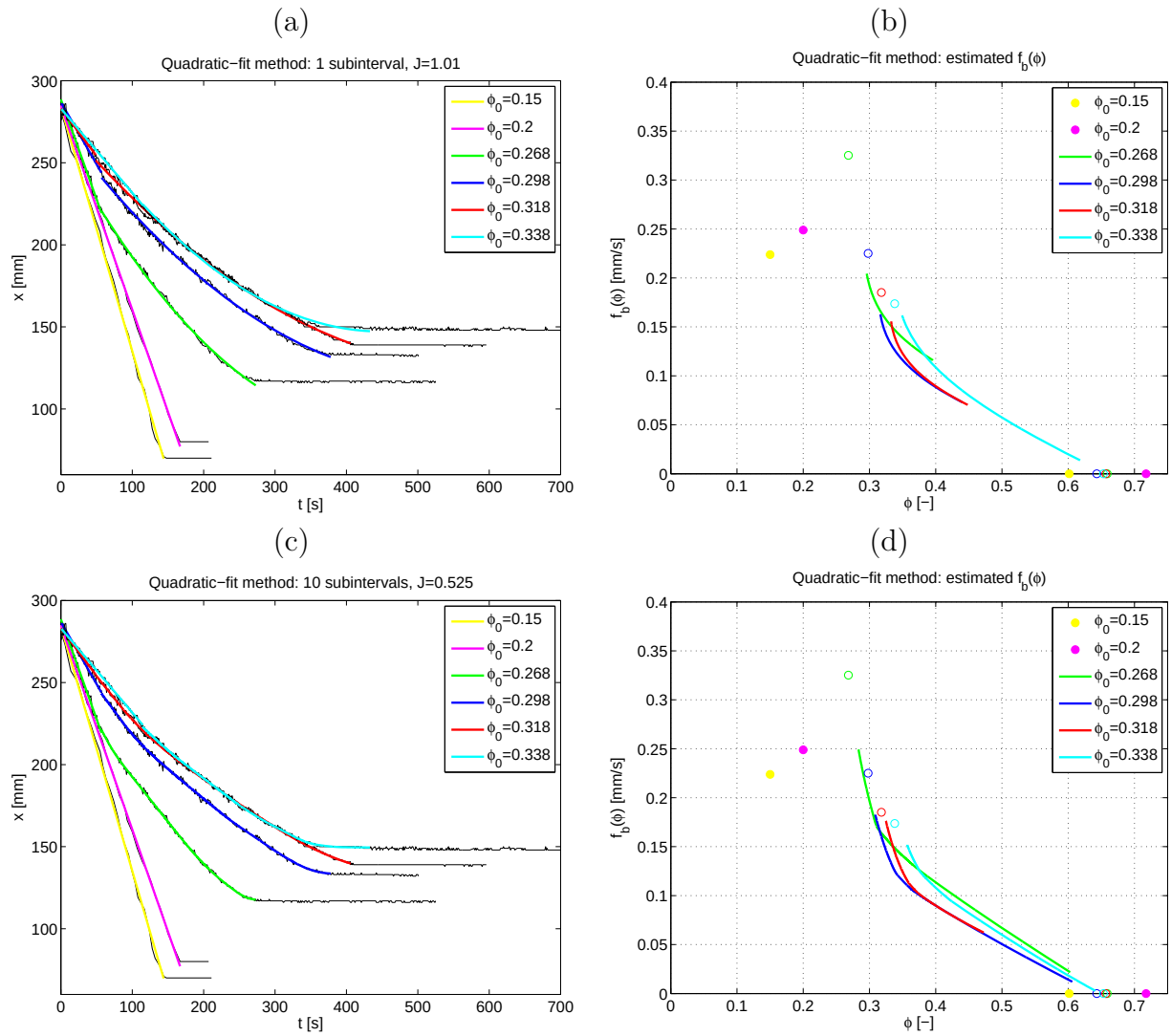

FIGURE 11. Flux identification from six Kynch tests of a suspension of glass beads in glycerine with the quadratic-fit method with (a, b) $n = 1$ and (c, d) $n = 10$. In (a, c), the experimental data for the suspension-supernate interfaces are shown as black curves and the coloured straight lines and curves the reconstructed interfaces. In (b, d), the identified portions $\check{f}_{\mathrm{b}}$ are shown plus isolated approximate values of f_{b} coming from the observation of initial settling velocities.

The same coefficients also arise in the formula for identified segment $\check{f}_{\mathrm{b}}$ of f_{b},

$$\check{f}_{\mathrm{b}}(\phi) = -\Big(b_1\phi + 2\big(a_1\phi(c_1\phi - H\phi_0)\big)^{1/2}\Big) \quad \text{for } \frac{H\phi_0}{\check{\eta}(t_1)} < \phi \leqslant \frac{H\phi_0}{\check{\eta}(t_N)},$$

which follows from formula (A.5) in the Appendix by setting $n = 1$.

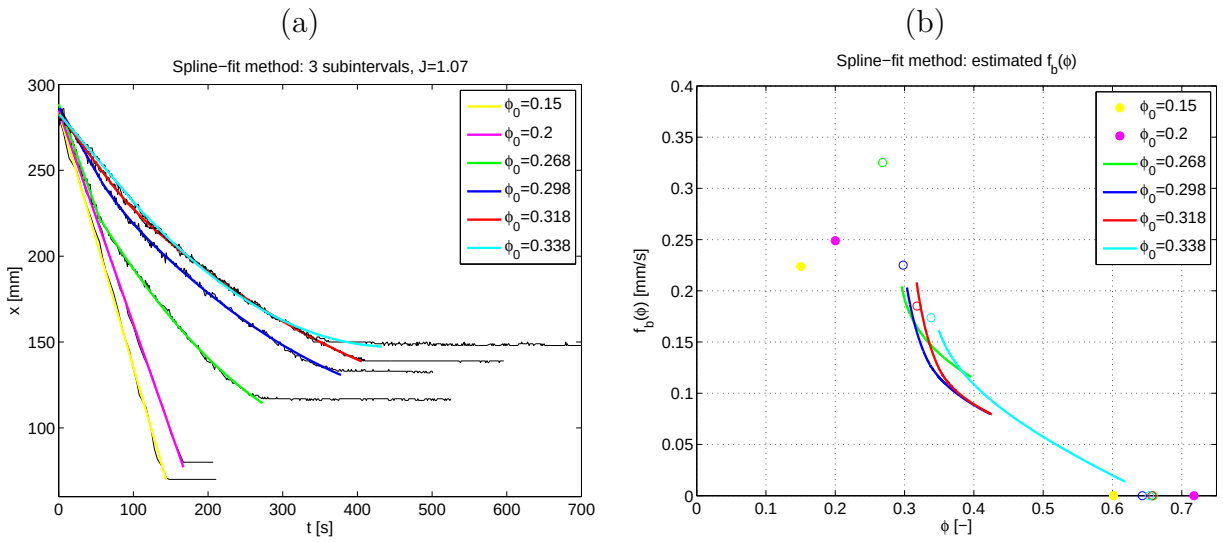

FIGURE 12. Flux identification from Kynch tests of a suspension of glass beads in glycerine with the spline-fit method with $n = 3$, showing (a) the reconstructed suspension-supernate interfaces and (b) the identified portions $\check{f}_{\mathrm{b}}$, plus isolated approximate values of f_{b} coming from the observation of initial settling velocities.

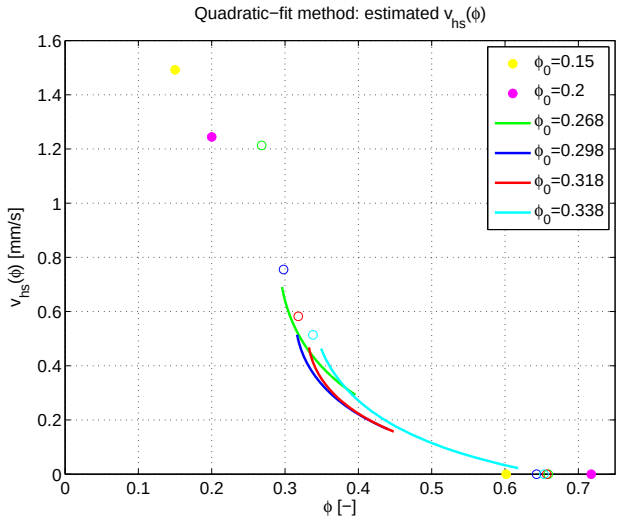

FIGURE 13. Estimation of the settling velocity $v_{\mathrm{hs}}(\phi)$ based on the data of Figure 11 (b).

The coefficients for the spline-fit method (22) for the same value $\phi_0 = 0.338$ with one interval are

$$a_1 = -1.0000 \times 10^{-10}, \quad b_1 = 6.9327 \times 10^{-4}, \quad c_1 = -0.6225, \quad d_1 = 286.9583.$$

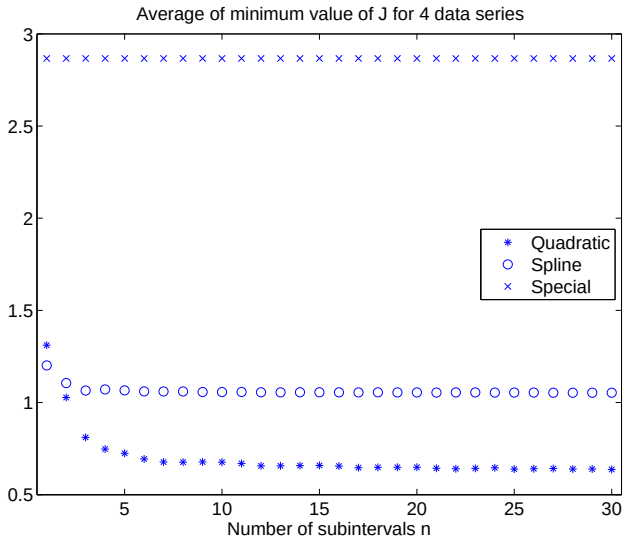

FIGURE 14. Average minimum values of the functional J_{total} for each fixed number of subintervals n.

In the case of the spline-fit, the convexity constraint is $a_i < 0$ for $i = 1, \ldots, n$ (Bürger and Diehl, 2013). Since this parameter is almost zero ($-a_1 = \varepsilon = 10^{-10}$, see the Appendix), the best fit is in fact a quadratic function. The reason that the quadratic function gives a better fit, i.e. gives a lower value of J, is that there are no constraints on the second derivative in the optimization. According to Theorem 2.1 of Bürger and Diehl (2013), this means that the resulting estimated portion of the flux is only once continuously differentiable.

ACKNOWLEDGEMENT

FB acknowledges support by Conicyt Programm "Inserción de Capital Humano en la Academia" 791100041. RB and CM are supported by Fondecyt project 1130154. Moreover, RB is supported by BASAL project CMM, Universidad de Chile and Centro de Investigación en Ingeniería Matemática (CI^{2}MA), Universidad de Concepción; Conicyt project Anillo ACT1118 (ANANUM); and Red Doctoral REDOC.CTA, MINEDUC project UCO1202 at Universidad de Concepción.

APPENDIX

For the quadratic-fit, the regularity constraint implies that the curve (21) must be differentiable, which means that at the points t_{j_i}, $i = 2, \ldots, n$, the neighboring segments $\check{h}_{i-1}$ and $\check{h}_i$ must have the same value and derivative, i.e., we impose

$$\check{h}_{i-1}(t_{j_i}) = \check{h}_i(t_{j_i}), \quad i = 2, \ldots, n, \tag{A.1}$$

$$\check{h}'_{i-1}(t_{j_i}) = \check{h}'_i(t_{j_i}), \quad i = 2, \ldots, n. \tag{A.2}$$

Inserting the functional form (23) into (A.1) and (A.2) we obtain the equality constraint $\boldsymbol{R}^{\mathrm{quad}}\boldsymbol{p} = \boldsymbol{0}$, where

$$\boldsymbol{R}^{\mathrm{quad}} = \begin{bmatrix} \boldsymbol{R}_2 & -\boldsymbol{R}_2 & \boldsymbol{0} & \cdots & \boldsymbol{0} \\ \boldsymbol{0} & \boldsymbol{R}_3 & -\boldsymbol{R}_3 & \ddots & \vdots \\ \vdots & \ddots & \ddots & \ddots & \boldsymbol{0} \\ \boldsymbol{0} & \cdots & \boldsymbol{0} & \boldsymbol{R}_n & -\boldsymbol{R}_n \end{bmatrix}, \quad \text{where} \quad \boldsymbol{R}_i = \begin{bmatrix} \boldsymbol{q}(t_{j_i})^{\mathrm{T}} \\ \boldsymbol{q}'(t_{j_i})^{\mathrm{T}} \end{bmatrix}, \quad i = 2, \dots, n.$$

Furthermore, the convexity constraints, namely

$$\check{h}_i''(t) > 0 \quad \text{for } t_{j_i} \leqslant t < t_{j_{i+1}},\ i = 1, \dots, n, \quad \text{and} \quad \check{h}_n''(t_n) \geqslant 0,$$

applied to the functional form (23) imply $a_i > 0$ for $i = 1, \dots, n-1$ and $a_n \geqslant 0$. However, we impose the constraint $a_i > 0$ for $i = 1, \dots, n$. These conditions are expressed as $\boldsymbol{I}^{\mathrm{quad}}\boldsymbol{p} \leqslant \boldsymbol{b}^{\mathrm{quad}}$, where the $(n+1) \times (4n)$ matrix $\boldsymbol{I}^{\mathrm{quad}}$ is defined by

$$\boldsymbol{I}^{\mathrm{quad}} = \begin{bmatrix} -\boldsymbol{e}_1^{\mathrm{T}} & \boldsymbol{0} & \dots & \boldsymbol{0} \\ \boldsymbol{0} & -\boldsymbol{e}_1^{\mathrm{T}} & \ddots & \vdots \\ \vdots & \ddots & \ddots & \boldsymbol{0} \\ \boldsymbol{0} & \cdots & \boldsymbol{0} & -\boldsymbol{e}_1^{\mathrm{T}} \\ 0 & \cdots & 0 & \boldsymbol{q}'(t_N)^{\mathrm{T}} \end{bmatrix}, \quad \text{where} \quad \boldsymbol{e}_1 = \begin{pmatrix} 1 \\ 0 \\ 0 \\ 0 \end{pmatrix},$$

and we set $\boldsymbol{b} := -\varepsilon(1, \dots, 1, 0)^{\mathrm{T}}$, where $\varepsilon > 0$ is a small parameter.

With the ingredients specified above for the quadratic-fit method, we can solve the constrained quadratic programming problem (25) (for this task, standard software packages are available) to obtain the coefficients of the functions $\check{h}_i(t)$, $i = 1, \dots, n$.

We then get that the function $\check{\eta}$ defined in (17) is defined analogously to (21), namely by

$$\check{\eta}(t) = \sum_{i=1}^{n} \check{\eta}_i(t)\chi_i(t) \quad \text{for } t_1 < t \leqslant t_N,$$

where $\check{\eta}_i(t) := \check{h}_i(t) - t\check{h}_i'(t) = -a_i t^2 + c_i$ for $i = 1, \dots, n$. The desired portion of $\check{f}_{\mathrm{b}}$ is calculated from (18), which requires that we calculate the inverse $\check{\eta}^{-1}$ of $\check{\eta}$. To this end, we first define the characteristic functions

$$\psi_i(\phi) := \begin{cases} 1 & \text{if } \check{\eta}(t_{j_{i+1}}) \leqslant H\phi_0/\phi < \check{\eta}(t_{j_i}), \\ 0 & \text{otherwise,} \end{cases} \quad i = 1, \dots, n. \tag{A.3}$$

For the quadratic-fit, we obtain that each of the functions $\check{\eta}_i(t)$ has the inverse

$$\check{\eta}_i^{-1}(y) = \left(\frac{c_i - y}{a_i}\right)^{1/2} \quad \text{for } \check{\eta}(t_{j_{i+1}}) \leqslant y < \check{\eta}(t_{j_i}), \tag{A.4}$$

so that inserting $y = H\phi_0/\phi$ into (A.4) and taking into account (A.3), we obtain from (18) the explicit formula

$$\check{f}_{\mathrm{b}}(\phi) = -\sum_{i=1}^{n} \Big(b_i\phi + 2\big(a_i\phi(c_i\phi - H\phi_0)\big)^{1/2} \Big) \psi_i(\phi) \quad \text{for } \frac{H\phi_0}{\check{\eta}(t_1)} < \phi \leqslant \frac{H\phi_0}{\check{\eta}(t_N)}. \tag{A.5}$$

References

Aziz, A.A.A., de Kretser, R.G., Dixon, D.R. and Scales, P.J., 2000. The characterisation of slurry dewatering. Water Science and Technology 41(8), 9–16.

Barton, N.G., Li, C.-H. and Spencer, S.J., 1992. Control of a surface of discontinuity in continuous thickeners. Journal of the Australian Mathematical Society Series B 33, 269–289.

Becker, R., 1982. Espesamiento Continuo, Diseño y Simulación de Espesadores. Habilitación Profesional, Universidad de Concepción, Chile.

Berres, S., Bürger, R., Karlsen, K.H. and Tory, E.M., 2003. Strongly degenerate parabolic-hyperbolic systems modeling polydisperse sedimentation with compression. SIAM Journal on Applied Mathematics 64, 41–80.

Betancourt, F., Concha, F. and Sbárbaro, D. (2013) Simple mass balance controllers for continuous sedimentation. Computers & Chemical Engineering 54, 34–43.

Bueno, J.L., Coca, J., Cuesta, E., Gutierrez Lavin, A. and Velasco, G., 1990. Sedimentation of coal slurries: a procedure for the determination of the flocculated-solid flux curve useful for the design of continuous settling tanks. Powder Technology 63, 133–140.

Bürger, R., Coronel, A. and Sepúlveda, M., 2009. Numerical solution of an inverse problem for a scalar conservation law modelling sedimentation. In: Tadmor, E., Liu, J.-G. and Tzavaras, A.E. (editors), *Hyperbolic Problems: Theory, Numerics and Applications*. Proceedings of Symposia in Applied Mathematics, Vol. 67, Part 2, pp. 445–454. American Mathematical Society, Providence, RI, USA.

Bürger, R. and Diehl S., 2013. Convexity-preserving flux identification for scalar conservation laws modelling sedimentation. Inverse Problems 29, paper 045008 (30pp).

Bürger, R., Diehl, S. and Nopens, I., 2011. A consistent modelling methodology for secondary settling tanks in wastewater treatment. Water Research 45, 2247–2260.

Bürger, R., Diehl, S., Farås, S. and Nopens, I., 2012. On reliable and unreliable numerical methods for the simulation of secondary settling tanks in wastewater treatment. Computers & Chemical Engineering 41, 93–105.

Bürger, R., Diehl, S., Farås, S., Nopens, I. and Torfs, E., 2013. A consistent modelling methodology for secondary settling tanks: a reliable numerical method. Water Science and Technology, to appear.

Bürger, R., Karlsen, K.H., Risebro, N.H. and Towers, J.D., 2004. Well-posedness in BV_t and convergence of a difference scheme for continuous sedimentation in ideal clarifier-thickener units. Numerische Mathematik 97, 25–65.

Bürger, R., Karlsen, K.H. and Towers, J.D., 2005a. A model of continuous sedimentation of flocculated suspensions in clarifier-thickener units. SIAM Journal on Applied Mathematics 65, 882–940.

Bürger, R., Karlsen, K.H. and Towers, J.D., 2005b. Mathematical model and numerical simulation of the dynamics of flocculated suspensions in clarifier-thickeners. Chemical Engineering Journal 111, 119–134.

Bürger, R., Karlsen, K.H., Torres, H., and Towers, J.D., 2010. Second-order schemes for conservation laws with discontinuous flux modelling clarifier-thickener units. Numerische Mathematik 116, 579–617.

Bürger, R. and Narváez, A., 2007. Steady-state, control, and capacity calculations for flocculated suspensions in clarifier-thickeners. International Journal of Mineral Processing 84, 274–298.

Bustos, M.C., Concha, F., Bürger, R. and Tory, E.M., 1999. Sedimentation and Thickening, Kluwer Academic Publishers, Dordrecht, The Netherlands.

Chancelier, J.P., Cohen de Lara, M., and Pacard, F., 1994. Analysis of a conservation PDE with discontinuous flux: A model of settler. SIAM Journal on Applied Mathematics 54, 954–995.

Coe, H.S., Clevenger, G.H., 1916. Methods for determining the capacities of slime settling tanks. Transactions of the American Institute of Mining Engineers 55, 356–385.

Coronel, A., James, F. and Sepúlveda, M., 2003. Numerical identification of parameters for a model of sedimentation processes. Inverse Problems 19, 951–972.

De Kretser, R.G., Usher, S.P., Scales, P.J., Boger, D.V. and Landman, K.A., 2001. Rapid filtration measurement of dewatering design and optimization parameters. AIChE Journal 47, 1758–1769.

Diehl, S., 1996. A conservation law with point source and discontinuous flux function modelling continuous sedimentation. SIAM Journal on Applied Mathematics 56, 388–419.

Diehl, S., 2007. Estimation of the batch-settling flux function for an ideal suspension from only two experiments. Chemical Engineering Science 62, 4589–4601.

Diplas, P. and Papanicolaou, A.N., 1997. Batch analysis of slurries in zone settling regime. Journal of Evironmental Engineering 123, 659–667.

Font, R. and Laveda, M.L., 2000. Semi-batch test of sedimentation. Application to design. Chemical Engineering Journal 80, 157-165.

Garrido, P., Bürger, R. and Concha, F., 2000. Settling velocities of particulate systems: 11. Comparison of the phenomenological sedimentation-consolidation model with published experimental results. International Journal of Mineral Processing 60, 213–227.

Garrido, P., Burgos, R., Concha, F. and Bürger, R., 2003. Software for the design and simulation of gravity thickeners. Minerals Enginering 16, 85–92.

Grassia, P., Usher, S.P. and Scales, P.J., 2008. A simplified parameter extraction technique using batch settling data to estimate suspension material properties in dewatering applications. Chemical Engineering Science 63, 1971–1986.

Grassia, P., Usher, S.P. and Scales, P.J., 2011. Closed-form solutions for batch settling height from model settling flux functions. Chemical Engineering Science 66, 964–972.

Karamisheva, R.D. and Islam, M.A., 2005. Development of a new model for batch sedimentation and application to secondary settling tanks design. Water Environment Research 77, 3066–3073.

Kynch, G.J., 1952. A theory of sedimentation. Transactions of the Faraday Society 48, 166–176.

Lester, D.R., 2002. Colloidal Suspension Dewatering Analysis. Ph.D. thesis, Department of Chemical Engineering, University of Melbourne.

Lester, D.R., Usher, S.P. and Scales, P.J., 2005. Estimation of the hindered settling function $R(\phi)$ from batch-settling tests. AIChE Journal 51, 1158-1168.

Lev, O., Rubin, E. and Sheintuch, M., 1986. Steady state analysis of a continuous clarifier-thickener system, AIChE Journal 32, 1516–1525.

Nocoń, W., 2006. Mathematical modelling of distributed feed in continuous sedimentation. Simulation Modelling Practice and Theory 14, 493–505.

Richardson, J.F. and Zaki, W.N., 1954. Sedimentation and fluidization: part I. Transactions of the Institution of Chemical Engineers (London) 32, 35–53.

Talmage, W.P., Fitch, E.B., 1955. Determining thickener unit areas. Industrial and Engineering Chemistry 47, 38–41.

Usher, S.P., de Kretser, R.G, and Scales, P.J., 2001. Validation of a new filtration technique for dewaterability characterization. AIChE Journal 47, 1561–1570.

Wilhelm, J.H., Naide, Y., 1981. Sizing and operating continuous thickeners. Mining Engineering 33, 1710–1718.

Wills, B.A. and Napier-Munn, T. (eds.), 2006. Wills' Mineral Processing Technology. Seventh Edition. Butterworth-Heinemann/Elsevier, Oxford, UK.

Centro de Investigación en Ingeniería Matemática (CI^{2}MA)

PRE-PUBLICACIONES 2013

2013-04 Tomás Barrios, Rommel Bustinza, Galina C. García, María González: *A posteriori error analyses of a velocity-pseudostress formulation of the generalized Stokes problem*

2013-05 Rodolfo Araya, Abner Poza, Frederic Valentin: *An adaptive residual local projection finite element method for the Navier-Stoker equations*

2013-06 Mohamed Helal, Erwan Hingant, Laurent Pujo-Menjouet, Glenn Webb: *Alzheimer's disease: Analysis of a mathematical model incorporating the role of prions*

2013-07 Ricardo Oyarzúa, Dominik Schötzau: *An exactly divergence-free finite element method for a generalized Boussinesq problem*

2013-08 Hernán Mardones, Carlos M. Mora: *Stable numerical methods for two classes of SDEs with multiplicative noise: bilinear and scalar*

2013-09 Alfredo Bermúdez, Dolores Gómez, Rodolfo Rodríguez, Pablo Venegas: *Mathematical and numerical analysis of a transient non-linear axisymmetric eddy current model*

2013-10 Ana Alonso-Rodriguez, Jessika Camaño, Rodolfo Rodríguez, Alberto Valli: *A posteriori error estimates for the problem of electrostatics with a dipole source*

2013-11 Zhixing Fu, Luis F. Gatica, Francisco J. Sayas: *Matlab tools for HDG in three dimensions*

2013-12 Salim Meddahi, David Mora, Rodolfo Rodríguez: *A finite element analysis of a pseudostress formulation for the Stokes eigenvalue problem*

2013-13 Gabriel Carcamo, Fabián Flores-Bazán: *A geometric characterization of strong duality in nonconvex quadratic programming with linear and nonconvex quadratic constraints*

2013-14 Raimund Bürger, Christophe Chalons, Luis M. Villada: *Anti-diffusive and random-sampling Lagrangian-remap schemes for the multi-class Lighthill-Whitham-Richards traffic model*

2013-15 Fernando Betancourt, Raimund Bürger, Stefan Diehl, Camilo Mejías: *Advance methods of flux identification for Clarifier-Thickener simulation models*

Para obtener copias de las Pre-Publicaciones, escribir o llamar a: Director, Centro de Investigación en Ingeniería Matemática, Universidad de Concepción, Casilla 160-C, Concepción, Chile, Tel.: 41-2661324, o bien, visitar la página web del centro: `http://www.ci2ma.udec.cl`







Centro de Investigación en
Ingeniería Matemática (CI²MA)
Universidad de Concepción

Casilla 160-C, Concepción, Chile
Tel.: 56-41-2661324/2661554/2661316
http://www.ci2ma.udec.cl